Modelling of the Vertical Dynamics of an Electric Kick Scooter

Michele Asperti[a], Michele Vignati[a] and Francesco Braghin[a]

[a] Politecnico di Milano, Department of Mechanical Engineering, Via La Masa 1, 20156 Milan, Italy

Abstract

Nowadays, micro-mobility is one of the major global trends in cities for the innovation of the transport system. In this context a breakthrough introduction of electric kick scooters (e-scooters) has taken place. Unfortunately, these mobility systems cause several accidents mainly for two reasons: wrong use and inadequate safety requirements. Since e-scooters are quite a new type of vehicle, generally accepted mathematical models are yet to be developed. These models can be useful in understanding the dynamical properties of this type of vehicle thus improving its design to reduce riding accidents. The present paper presents a model for the simulation of the vertical dynamic behavior of e-scooters that accounts also for the mechanical impedance of the driver, thus allowing to estimate the overall driver's comfort and road holding capabilities providing information on possible speed limitations in case of bad road conditions. Furthermore, the paper shows experimental envelope curves for lumped obstacles obtained with a dedicated test bench on which the e-scooter is fixed and tested under different conditions of vertical load and tire inflation pressure.

Keywords: Electric Scooter, Light Vehicles, Vehicle Modelling, Vehicle Dynamics, Comfort, Road Holding

1 Introduction

The use of computer simulations to fast up the design and to avoid risks and costs of experimental tests is a well-established technique in the passenger car industry, where both full-scale multibody and lumped parameter models are used. More recently computer simulations have been introduced in the motorcycle industry [1–3], where the task is much more complex if compared to cars since the vehicle itself is unstable and so it is not possible to simulate open loop maneuvers, a virtual rider is needed [4]. Furthermore, in passenger cars the mass of the driver is small if compared to the total mass of the system, thus it is possible to assume that any kind of driver model has only to properly control the vehicle inputs to perform closed-loop maneuvers while its inertial properties and motion can be neglected. Instead, in motorcycles the mass of the rider is an important part of the whole system mass and, moreover, he moves over the vehicle to drive it, thus influencing the dynamic properties of the whole system.

Regarding e-scooters, it should be noted that the simulation approach needs to be significantly different from the one adopted for cars and even motorcycles. In fact, for e-scooters the driver represents almost 90% of the total mass of the system and its dynamic properties significantly influence the overall dynamic behavior of the vehicle. This has been proven for bicycles, that show a driver/vehicle mass ratio like that of e-scooters, for which it has been demonstrated that the rider posture influences its comfort [5] and that the modal properties of the system with or without the rider change significantly [6].

When dealing with the modelling of any kind of mechanical system it is necessary to carefully select the level of detail of the model. A too coarse description of the system may result in an inadequate dynamic behavior, while a too detailed model makes it difficult to correctly measure or estimate the necessary parameters. Thus, the modelling of the e-scooter must be carried out considering the user as well as the variability of the user's inertial, stiffness and damping properties up to a reasonable level of detail.

Regarding human body modelling different approaches have been used through the years. When focusing on people motion, complete multibody models have been developed, where a certain number of joints and muscular tensions allows to correctly reproduce the biomechanics in dynamic simulations [7–9]. A completely different approach is used when inspecting the interaction between the human and the structures surrounding him. In this case where the interest is on the structures the human body model must be as simple as possible but it must correctly reproduce the interactions between the body and the structure. To accomplish this target lumped parameter models are used. In these models, the mass, stiffness and damping parameters do not correspond to any physical quantity of the human body but are tuned to show the same mechanical impedance behavior [10–15]. considerate is to point out that the mechanical impedance properties of the human body change with posture, the vibration magnitude, and the characteristics of each single subject [16–18].

Another crucial aspect of vehicle dynamic simulation is represented by tire modelling since the tire is the only element in contact with the ground and with which it exchanges the forces necessary to the motion. Through the years many models have been built for car tires and then some have recently been extended to motorcycle applications [19,20]. Among the wide variety of models one can mention FEM approaches that are really accurate especially when dealing with short wavelength obstacles but also require a long computational time. Another approach allowing good simulations on short wavelength obstacles is that of considering flexible tire models, where the belt is constituted several elements allowing to reproduce the deformation of the tire contact patch. Finnally, the most common approach considers a rigid ring tire that, to be used on short wavelength obstacles, requires a geometrical filter to be applied to the road unevenness to give as input to the model an effective surface that accounts for contact patch variation and obstacle enveloping properties [21].

Considering the high number of accidents involving e-scooters compared to the number of deployed vehicles, a standard has been recently introduced in Europe [22] that imposes safety requirements for all light motorized vehicle. A numerical model is thus necessary to properly guide the design process of this new type of vehicles.

This paper has the scope to study the dynamic behavior of e-scooters to provide hints about their design for reducing the number of accidents and improving their safety. The paper proposes a model for the study of the vertical dynamic behavior of e-scooters. It accounts for the mechanical impedance of the driver providing an important tool to estimate the overall driver's comfort and vehicle road holding capabilities. To correctly simulate the vehicle behavior when running over lumped obstacles, an experimental campaign has been carried out. The paper thus reports experimental data of some obstacles envelope curves for different normal loads and for several tire inflation pressures. These data are fed to the model to simulate the passage over concentrated obstacles. The overall model has been validated by comparing simulation results with experimental acceleration measurements. The paper thus provides an important tool that can be used to simulate the vehicle response and driver's comfort while running on several uneven road surfaces.

The paper is organized as follows. At first the road input modelling is introduced, then the definition of the e-scooter model is presented. Finally, after the tuning of the parameters of the model, its validation is performed by means of experimental tests.

2 Road modelling

The definition of the input coming from the road surface is of fundamental importance to effectively simulate the behavior of the e-scooter in common operating conditions. As it will be better detailed in the following section, the selected tire model is a single contact point model, requiring road inputs to be introduced in the simulation as imposed displacement to front and rear wheels ground contact points. This kind of model is extensively used since it is simple, and it results in good approximation of the tire forces when running over smooth road profiles characterized by wavelengths greater than the contact patch length. However, this model alone is not able to reproduce the tire enveloping behavior over obstacles that have a length close to that of the tire contact patch. Because of this reason it is necessary to distinguish between two different road inputs. The first is associated with road irregularity and can be given directly as input to the e-scooter model, while the second is associated with lumped obstacles which need to be somehow modified before being used as input to the model.

The road irregularity is modelled according to ISO 8608 standard [23] that defines 8 classes of road roughness profiles for simulation purposes basing on the Power Spectral Density (PSD) of the road irregularity.

In case of lumped obstacles, whose dimensions are comparable to the ones of the tire contact patch, the tire deformation makes the tire contact point displacement to be different from the real shape of the obstacle. The lumped obstacles are thus generally filtered before being fed to the single contact point tire models. This requires the definition of a filtering policy for short wavelength obstacles, that in many car applications is constituted by the elliptical tandem-cam model [21]. The definition of this model that geometrically filters the lumped obstacles requires in general a long series of quasi-static experiments and some sort of shape optimization procedures. In this article the geometrical filter is not defined but some short obstacles are considered and introduced in the simulations by means of their experimental quasi-static enveloping. Characterization tests are carried out using the experimental apparatus reported in **Figure 1**. The e-scooter is fixed to a frame at the front hub with the rear wheel free to move over a sled on which different obstacles are bolted. Making reference to **Figure 2,** the acquisition of the longitudinal displacement of the sled and of the vertical displacement of the wheel hub is made by means of laser sensors from which the tire enveloping behavior over the available obstacles is reconstructed. Obstacles geometric properties are reported in **Table 1**.

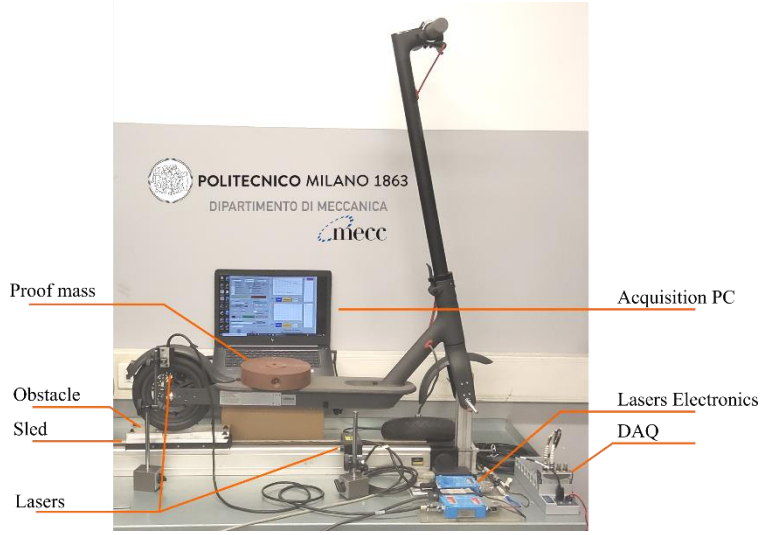

Figure 1. Experimental apparatus for tire enveloping characterization over short wavelength obstacles

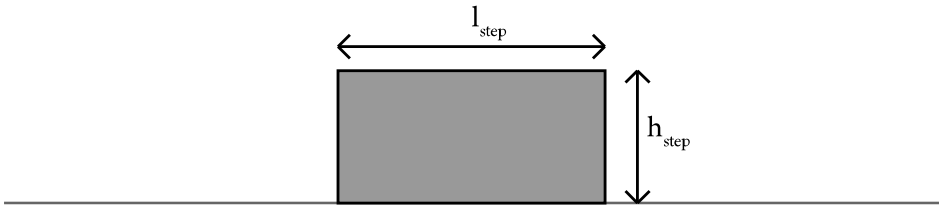

Figure 2. Obstacles geometry and reference geometric dimensions

Table 1. Obstacles geometric properties.

Obstacle	A	B	C
h_{step} [mm]	10	10	4
l_{step} [mm]	80	20	40

The acquisition of the tire envelope when engaging the obstacles is performed for different tire inflation pressures (1.5, 2.0 and 2.5 bar) and for various loading conditions (0-90 kg) by increasing the e-scooter payload through metal disks placed in the deck center. The acquisition is performed running back and forth on the obstacle several times for each configuration. Obtained data are fit with a piecewise cubic Hermite interpolating polynomial that allows to obtain a smooth obstacle envelope. A preliminary result of this procedure is reported in **Figure 3**. It reports enveloping results for obstacles A and B for a tire inflation pressure of 2.0 and 2.5 bars and a deck load of 50 and 90 kg as detailed in the figure.

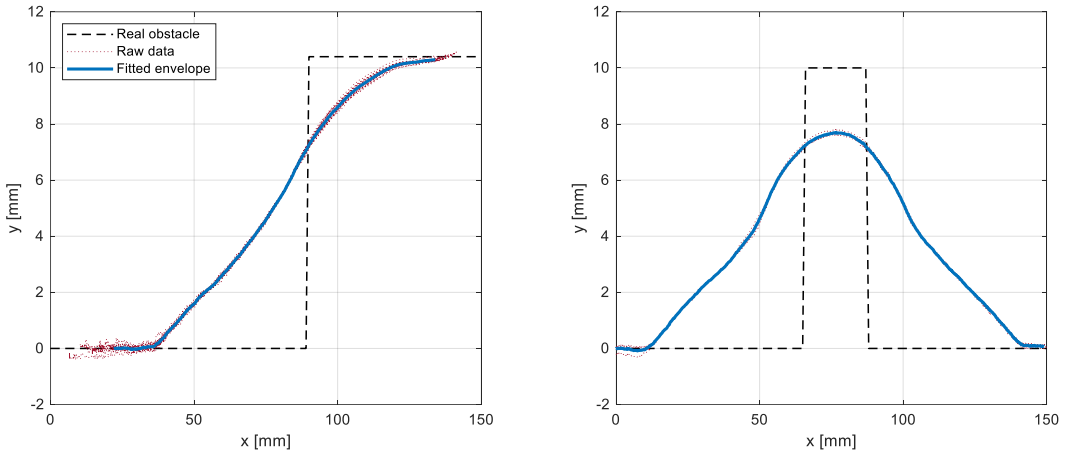

Figure 3. Tire enveloping characteristics on obstacles. Left: Up-step phase on A lumped obstacle with an inflation pressure of 2.5 bar and a deck load of 90 kg. Right: Complete passage on B lumped obstacle with an inflation pressure of 2.0 bar and a deck load of 50 kg

Once clear how the smooth obstacle envelope has been obtained it is possible to look at how different values of tire inflation pressure and deck loading are influencing the enveloping behavior on lumped obstacles.

2.1 Obstacle A

Figure 4 reports experimental results for the up-step phase of the tire on lumped obstacle A, considering deck loads of 50 kg, 70 kg, and 90 kg and an inflation pressure of 1.5 bar (**Figure 4.a**) and 2.0 bar (**Figure 4.b**). This obstacle can be considered as a step since it is longer than the tire contact patch length. Thanks to this, the final vertical displacement of the wheel hub is not affected by tire inflation pressure or vertical load since the contact patch is the same before and above the obstacle. This is reasonable since, with a fixed vertical load of the wheel hub, the loaded tire radius should not be different if on the ground or on the obstacle.

Looking at the results obtained at the two inflation pressures (**Figure 4.a** and **Figure 4.b**) it is clear that in both cases for an increasing payload on the e-scooter deck the enveloping starts earlier. This happens since at a constant inflation pressure the contact patch gets bigger as the load increases and so the first contact with the obstacle happens at a greater longitudinal distance from the wheel hub. Regarding the shape of the envelopes, it can be noticed that an increasing load generates a smoother curve at the first and last stages, while the intermediate one is superimposed, no matter of which the vertical load is.

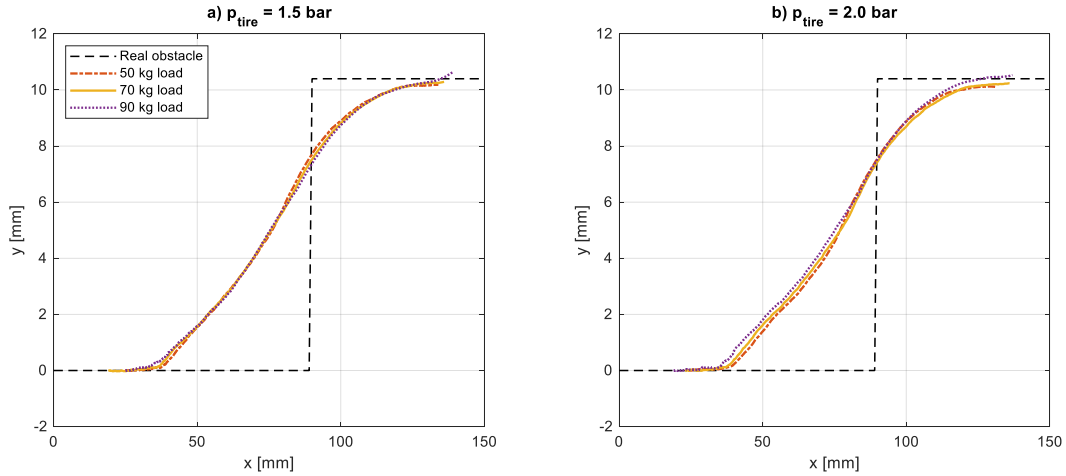

Figure 4. Tire enveloping characteristics on A lumped obstacle up-step phase. Comparison of fitted envelopes at different tires inflation pressures and deck loading

2.2 Obstacle B

Figure 5 reports experimental results for the full envelope on lumped obstacle B, considering deck loads of 50 kg, 70 kg, and 90 kg and an inflation pressure of 1.5 bar (**Figure 5.a**) and 2.5 bar (**Figure 5.b**). In this

case the obstacle length is shorter than tire contact patch length. In fact, it is so short that, when on top of the obstacle, the tire contact patch has the length of the obstacle itself. For this reason, in the middle of the obstacle, the height of the envelope decreases when increasing the vertical load, at constant inflation pressure, and when decreasing the inflation pressure, at constant vertical load.

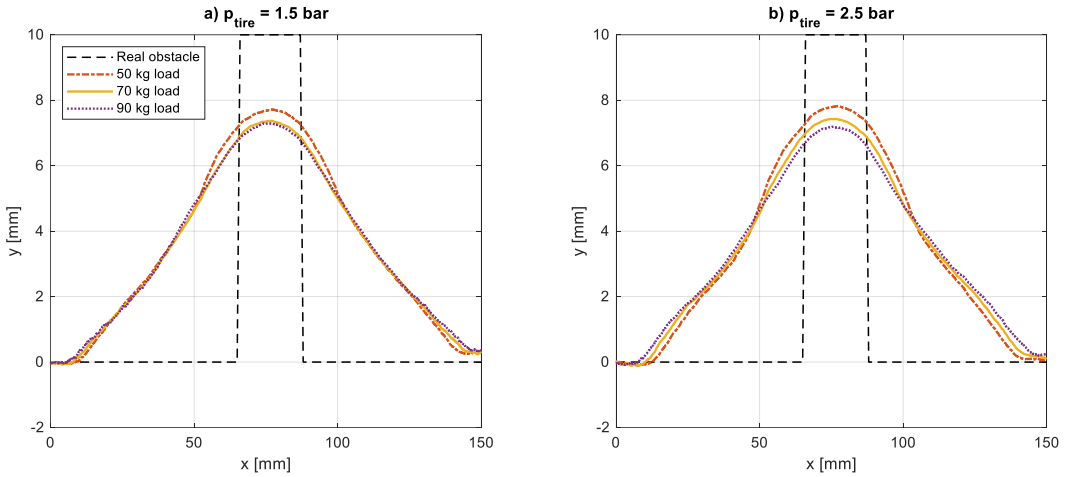

Figure 5. Tire enveloping characteristics on B lumped obstacle. Comparison of fitted envelopes at different tires inflation pressures and deck loading

2.3 Obstacle C

Figure 6 reports experimental results for lumped obstacle C considering deck loads of 50 kg, 70 kg and 90 kg and an inflation pressure of 2.0 bar in **Figure 6.a** and 2.5 bar in **Figure 6.b**. The same considerations drawn for obstacle B can be made in this case since it is still the case of an obstacle whose length is shorter than the tire contact patch length on a flat surface.

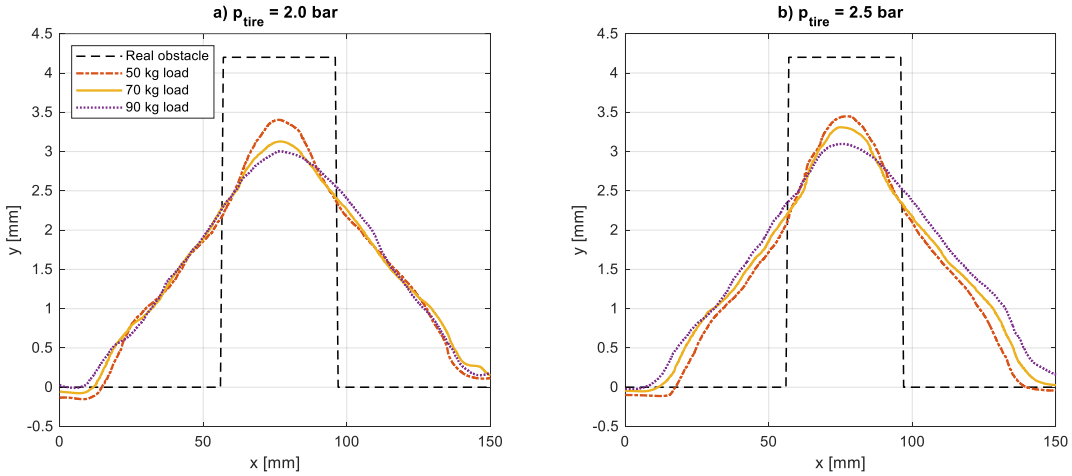

Figure 6. Tire enveloping characteristics on C lumped obstacle. Comparison of fitted envelopes at different tires inflation pressures and deck loading

3 E-scooter modelling

Both comfort and safety of the e-scooter are related to its vertical dynamics which influences the vibrations induced to the rider and the road holding capability of the wheels. To study the e-scooter vertical dynamics a lumped parameters model is defined. This approach is well known in literature for other vehicles, and it allows to get meaningful results without increasing the modeling complexity. The model developed in this work is shown in **Figure 7** and it is constituted by rider and tires subsystems assembled on a rigid e-scooter frame.

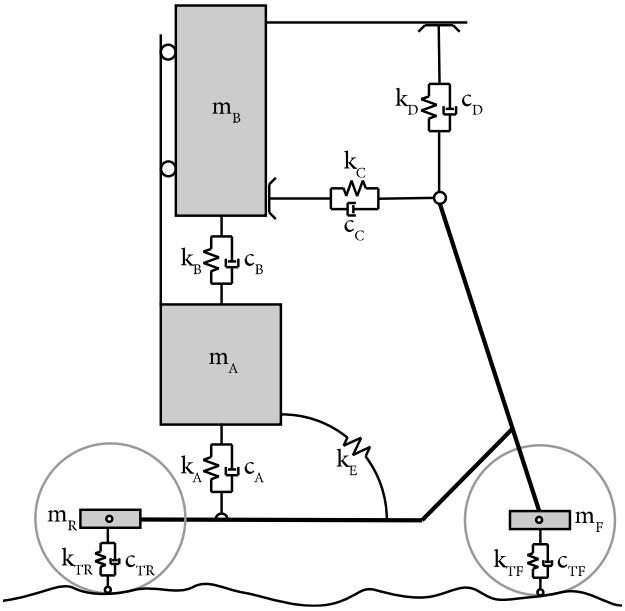

Figure 7. E-scooter lumped parameter model overview

3.1 Tire model

Tires are represented by means of a single contact point model, with road inputs introduced in the simulation as imposed displacement to front and rear wheels ground contact points. Stiffness and damping properties of the tire are reproduced using a spring-damper element that accounts for the tire radial stiffness and damping. The tire static radial stiffness is obtained using the same experimental setup as for obstacle enveloping purposes, where the sled is kept fixed, and no obstacles are mounted on it. The procedure for the identification of the tire radial stiffness is performed for different tire inflation pressures (1.5, 2.0, and 2.5 bar), for ten different loads positioned in the deck center, from 0 to 90 kg, as in the experimental setup previously described. By measuring the vertical load at the tire contact patch and the vertical displacement of the wheel hub, a cloud of points can be obtained. Experimental data, as from literature [24,25], are interpolated by means of a second order polynomial function that relates the hub force F_r to the radial deflection δ_r:

$$F_r = a_1\,\delta r + a_2\,\delta r^2 \tag{5}$$

From previous expression, the tire radial stiffness k_r is obtained by analytically deriving the force expression with respect to the deflection:

$$k_r = a_1 + 2\,a_2\,\delta r \tag{6}$$

Figure 8 shows experimental results and fitting curve for the tire inflation pressure of 2.5 bar while **Table 2** reports the fitting coefficients for all the tested inflation pressure values. The obtained stiffness is then used in the tire single contact point model within the full e-scooter model. Instead, for what concerns the radial damping of the tire, the value is taken from literature for bicycle tires whose shape and dimension are like the ones of those mounted on e-scooters.

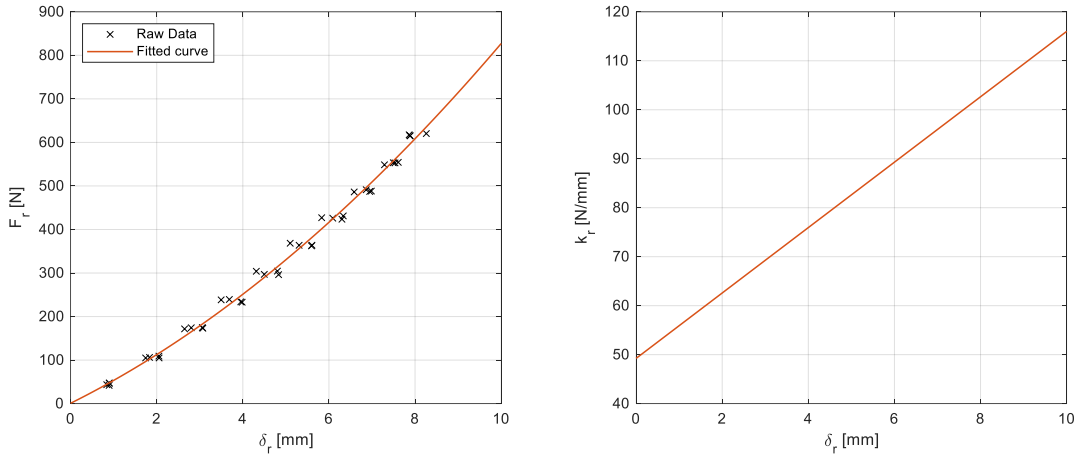

Figure 8. Tire radial characteristics. Left: Tire radial force as function of tire radial deflection. Right: Tire radial stiffness as function of tire radial deflection

Table 2. Tire radial force VS radial deflection fitting parameters.

Inflation pressure [bar]	a_1 [N/mm]	a_2 [N/mm^2]
1.5	15.8	4.16
2.0	35.4	3.37
2.5	49.2	3.34

3.2 Rider model

In the modelling phase it is assumed that the position of the rider over the deck is fixed and that there is no feedback from him. This approach is reasonable when simulating the vertical dynamics in a condition mainly associated with straight running, where the rider does not move his feet over the deck, and he is not acting on the handlebars to change direction or to correct the trajectory. These assumptions are the ones allowing to use a standard 2 DOFs impedance model for the standing human body exposed to vertical whole-body vibrations [12]. Since both vehicle and rider are not only moving vertically but are also pitching for some amount, a rotational elastic element is introduced between the e-scooter deck and the rider lower mass to account for the ankle stiffness, that is obtained from [26].

The 2 DOFs impedance model for the standing human body exposed to vertical whole-body vibrations retrieved from [12] is not defined for the specific application of this article but at least gives some initial guess parameters for the model considering three postures that can be assumed by rider. Among these, the posture referred as normal standing is the closest to the one normally assumed by a human being when riding an e-scooter. Instead, the postures referred as legs-bent standing or one-leg standing are only occasionally assumed by e-scooter riders and mainly in conditions involving out-of-plane maneuvers of the vehicle like when engaging a turn. For the scope of the work, in which straight running of the e-scooter is considered, it is reasonable to start from the parameters of the impedance model of the normal standing human body and eventually tune them to achieve a correct reproduction of the dynamics of the whole system. At this stage it is important to highlight that the masses, springs, and dampers used to build such kind of models do not correspond to any physiological structure within the human body, but the goal is to reproduce the drive point mechanical impedance for a wide range of frequencies.

Regarding the effects of the human hand-arm system on the handlebar, the model is derived from the 2 DOFs mechanical impedance model (Annex B – Model 1) from [27] that considers the same schematization for three directions of applications relative to the human hand, where lumped parameters are adopted to fit the model as shown in the following. Model from [27] has been built and validated for vibrations but in the current application the motion amplitude is quite large. This requires a simplification of the hand-arm system allowing to correctly reproduce the forces exchanged at the handlebar. Only two directions are of interest, the vertical and the longitudinal ones, for which the 2 DOFs models have been substituted by spring and damper elements in parallel (see **Figure 9**). This approach guarantees the reproduction of the hand-arm system static stiffness starting from a validated set of data and the schematics of this procedure is reported in **Figure 9**, where both the original and the simplified model are reported.

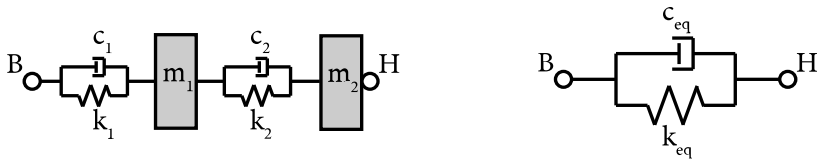

Figure 9. Hand-arm system models with H indicating the handle side and B indicating the body side. Left: Original full-scale model. Right: Simplified model

The procedure of switching from the original to the simplified model basically consists in neglecting the masses and calculating the equivalent stiffness and damping considering that the elements are put in series.

$$k_{eq} = \frac{k_1\, k_2}{k_1 + k_2} \tag{7}$$

$$c_{eq} = \frac{c_1\, c_2}{c_1 + c_2} \tag{8}$$

Referring to the model scheme of **Figure 7**, the resulting parameters for the simplified hand-arm system model are reported in **Table 3**.

Table 3. Driver hand-arm system model characteristic parameters

Parameter	Value
k_C [N/m]	800
k_D [N/m]	2000
c_C [Ns/m]	40
c_D [Ns/m]	125

Knowing the huge effect of posture on the mechanical impedance of the standing human body [17,18], the tuning of the body parameters is carried out by running an experimental campaign in which some quantities representing the real dynamics of the vehicle plus driver have been measured. For this reason, an e-scooter without suspensions has been equipped with 6 mono-axial accelerometers (see **Figure 10**). Vertical accelerations have been acquired at both front and rear wheel hubs, deck center and handlebar. Longitudinal accelerations have been acquired only at the front wheel hub and at the center of the handlebar. To directly compare experimental and numerical results, the system needs to be excited in the same way in the experiments and in the computer simulations and so the lumped obstacle named as A is chosen as input. The tuning of the driver body model parameters is carried out considering a running speed of about 19 km/h and tires inflation pressure of 2.5 bar. The parameters that have been tuned are the ones listed in **Table 4.**

Figure 10 Experimental setup: location of accelerometers for the acquisition of accelerations when passing over a lumped obstacle

For the tuning of the driver body model parameters, the physical quantities that have been considered are the frequency and the decay of the vertical acceleration response at each wheel hub when that single tire is engaging the obstacle. Instead, the excitation caused on the opposite wheel that is not engaging the obstacle is not considered at this stage. The results obtained at the end of the tuning procedure in terms of vertical acceleration at both front and rear wheel hubs are reported in **Figure 11**, where experimental (dotted lines) and numerical (solid lines) time histories are directly compared.

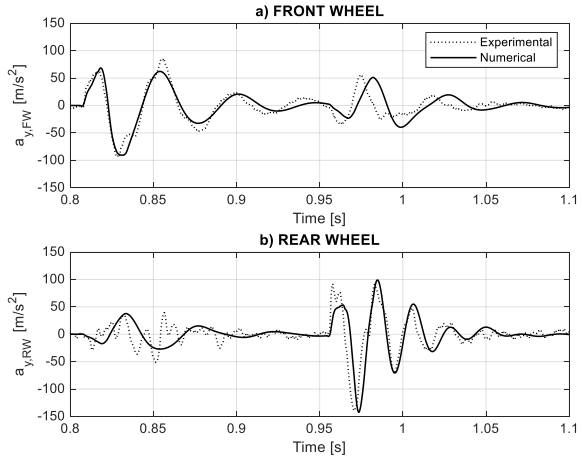

Figure 11. Comparison between experimental and numerical vertical accelerations at wheel hubs at the end of the driver body model parameters tuning passing over B lumped obstacle at a speed of about 19 km/h

In general, a good agreement can be observed: the vertical acceleration of the front and rear wheel centers is correctly reproduced by the model and the passing over the obstacle can be clearly identified. The front wheel passes over the obstacle at about 0.81 s while the rear wheel hits it at about 0.96 s. Moreover, it is important to highlight that the parameters of the driver body have been tuned considering a normalization on the driver own weight to be applicable independently of the mass (M) of the driver itself. The parameters resulting from this procedure and used throughout the work are reported in **Table 4**.

Table 4. Driver body model characteristic parameters

Parameter	Value
m_A [kg]	0.554 * M
m_B [kg]	0.456 * M
k_A [N/m]	4.39e3 * M
k_B [N/m]	5.53e2 * M
c_A [Ns/m]	3.99 * M
c_B [Ns/m]	4.37 * M

4 Model validation

Once the model has been tuned in a particular maneuver, it is important to validate it be checking the model performance in conditions that are different from the ones in which it has been tuned. Thus, further experimental maneuvers are run passing over the lumped obstacles previously described in the road modelling section. The use of lumped obstacles over general road unevenness allows to correctly reproduce the tire inputs in the simulations since that quantity has been directly measured, making the outputs of the computer simulations directly comparable with the experimental acquisitions.

Different conditions have been simulated always with the same rider but changing the obstacle, the tire inflation pressure, and the running speed. As an example, **Figure 12** shows the vertical acceleration response at most relevant points of the e-scooter, i.e. the wheel hubs, the deck center, and the handlebar, when passing over obstacle A with tires inflation pressure of 2.0 bar and a forward speed of about 17 km/h. As for previously presented results, simulation results in solid lines are compared to experimental measurements in dotted lines. Although the model has not been specifically tuned for the specific running speed and obstacle, a good agreement can be noticed. It can be clearly identified that the front wheel gets in contact with the obstacle at about 0.90 s, while the rear wheel at about 1.07 s. The vertical acceleration of the front and rear wheel hubs, **Error! Reference source not found.Figure 12.a** and **Figure 12.b**, is correctly reproduced by the model as

well as the vertical acceleration of the deck and handlebar center points, reported in **Figure 12.c** and **Figure 12.d** respectively. These last two quantities are important since they give the acceleration at the vehicle interface points with the driver, that are a direct indication of the comfort level perceived by the driver.

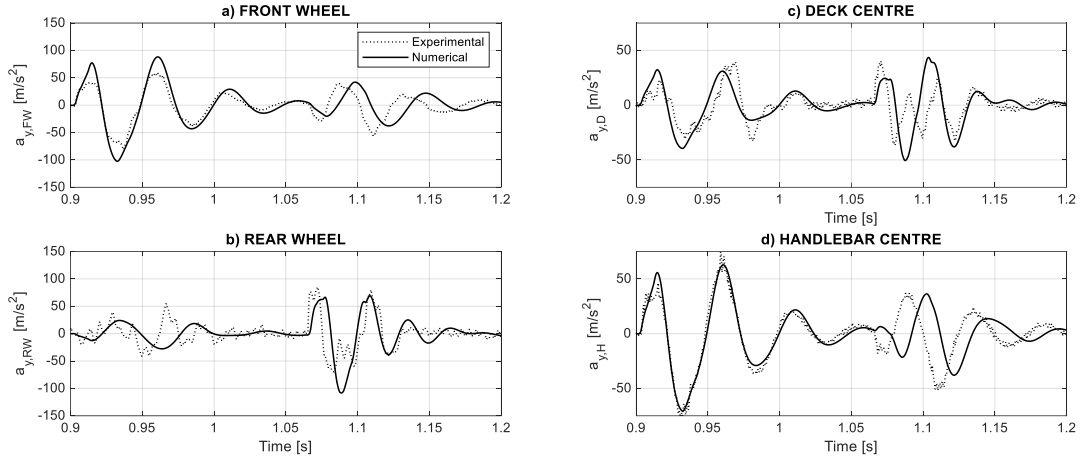

Figure 12. Comparison between experimental and numerical vertical accelerations at sensible points of the e-scooter passing over A lumped obstacle at a speed of about 17 km/h

To further prove the reliability of the model when passing over a lumped obstacle that has a different height than 10 mm, like obstacles A and B, simulations have been performed also getting over the C lumped obstacle. **Figure 13** shows the vertical acceleration response at the same sensible points previously mentioned, having the e-scooter running over the lumped obstacle C with tires inflation pressure of 2.5 bar and a forward speed of about 19 km/h. A general good agreement can be found between simulation results (solid lines) and experimental measurements (dotted lines). The vertical acceleration at both front and rear wheel centers, **Error! Reference source not found.Figure 13.a** and **Figure 13.b**, is correctly reproduced and their passing over the obstacle can be still clearly identified. The front wheel starts getting over the obstacle at about 0.81 s, while the real wheel at about 0.96 s. The vertical accelerations at deck and handlebar center points are respectively shown in **Figure 13.c** and **Figure 13.d**, where the simulation results still correctly reproduce the experimental measurements.

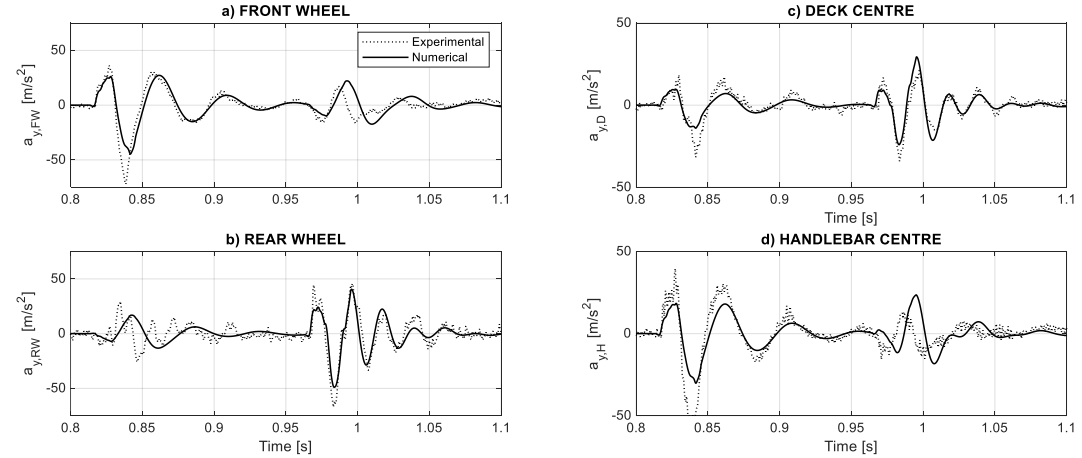

Figure 13. Comparison between experimental and numerical vertical accelerations at sensible points of the e-scooter passing over C lumped obstacle at a speed of about 19 km/h

5 Conclusions

The paper presents a planar model for the simulation of the vertical dynamics of an e-scooter. In particular, the model considers the mechanical impedance of the rider that deeply influences the dynamics of the whole system. Starting from common approaches in the modelling of the mechanical impedance of the human body for the excitation of structures, the necessary simplifications have been made to adapt them to the new scope. In addition, a pure assembling of different models developed with different purposes than those for which they

have been used in this article could not give satisfactory results and so parameters tuning has been part of the work. The lumped parameters characterizing the final model after the fine-tuning stage are still close to those which can be found in literature when inspecting various scenarios of application. Moreover, an experimental campaign has been run to acquire accelerations at relevant points on the e-scooter, that have shown to properly match with those reproduced by the simulation model.

This contribution gives an important tool for the design of e-scooters since, having a deeper understanding of the dynamics of the vehicle plus rider system, it will allow to define effective suspension geometries and tune their parameters to improve the road holding, but also to define some specific insulation layers between the frame and the rider at proper interface points in order to enhance the riding comfort level.

Funding: This research did not receive any specific grant from funding agencies in the public, commercial, or not-for-profit sectors.

References

[1] V. Cossalter, R. Lot, A motorcycle multi-body model for real time simulations based on the natural coordinates approach, Veh. Syst. Dyn. 37 (2002) 423–447. https://doi.org/10.1076/vesd.37.6.423.3523.

[2] V. Cossalter, R. Lot, F. Maggio, A multibody code for motorcycle handling and stability analysis with validation and examples of application, SAE Tech. Pap. (2003). https://doi.org/10.4271/2003-32-0035.

[3] L. Leonelli, N. Mancinelli, A multibody motorcycle model with rigid-ring tyres: Formulation and validation, Veh. Syst. Dyn. 53 (2015) 775–797. https://doi.org/10.1080/00423114.2015.1014820.

[4] A.A. Popov, S. Rowell, J.P. Meijaard, A review on motorcycle and rider modelling for steering control, Veh. Syst. Dyn. 48 (2010) 775–792. https://doi.org/10.1080/00423110903033393.

[5] A. Polanco, E. Marconi, L. Muñoz, D. Suárez, A. Doria, Effect of rider posture on bicycle comfort, Proc. ASME Des. Eng. Tech. Conf. 3 (2019) 1–8. https://doi.org/10.1115/DETC2019-97763.

[6] A. Doria, E. Marconi, P. Cialoni, Modal analysis of a utility bicycle from the perspective of riding comfort, Proc. ASME Des. Eng. Tech. Conf. 3 (2019) 1–8. https://doi.org/10.1115/DETC2019-97277.

[7] D.A. Winter, Biomechanics and Motor Control of Human Movement: Fourth Edition, 2009. https://doi.org/10.1002/9780470549148.

[8] W. Blajer, K. Dziewiecki, Z. Mazur, Multibody modeling of human body for the inverse dynamics analysis of sagittal plane movements, Multibody Syst. Dyn. 18 (2007) 217–232. https://doi.org/10.1007/s11044-007-9090-2.

[9] A. Kecskemethy, Multibody Dynamics of Biomechanical Models for Human Motion via Optimization, Multibody Dyn. (2007). https://doi.org/10.1007/978-1-4020-5684-0.

[10] N. Nawayseh, S. Hamdan, M. Bernardo-Filho, R. Taiar, Modelling the apparent mass of the standing human body under whole-body vibration training conditions, Proc. Inst. Mech. Eng. Part H J. Eng. Med. 234 (2020) 697–710. https://doi.org/10.1177/0954411920917311.

[11] L. Wei, M.J. Griffin, Mathematical models for the apparent mass of the seated human body exposed to vertical vibration, J. Sound Vib. 212 (1998) 855–874. https://doi.org/10.1006/jsvi.1997.1473.

[12] Y. Matsumoto, M.J. Griffin, Mathematical models for the apparent masses of standing subjects exposed to vertical whole-body vibration, J. Sound Vib. 260 (2003) 431–451. https://doi.org/10.1016/S0022-460X(02)00941-0.

[13] N. Nawayseh, M.J. Griffin, A model of the vertical apparent mass and the fore-and-aft cross-axis apparent mass of the human body during vertical whole-body vibration, J. Sound Vib. 319 (2009) 719–730. https://doi.org/10.1016/j.jsv.2008.05.030.

[14] M. Tarabini, S. Solbiati, B. Saggin, D. Scaccabarozzi, Apparent mass matrix of standing subjects exposed to multi-axial whole-body vibration, Ergonomics. 59 (2016) 1038–1049. https://doi.org/10.1080/00140139.2015.1108459.

[15] M. Tarabini, S. Solbiati, G. Moschioni, B. Saggin, D. Scaccabarozzi, Analysis of non-linear response of the human body to vertical whole-body vibration, Ergonomics. 57 (2014) 1711–1723. https://doi.org/10.1080/00140139.2014.945494.

[16] M.G.R. Toward, M.J. Griffin, Apparent mass of the human body in the vertical direction: Inter-subject variability, J. Sound Vib. 330 (2011) 827–841. https://doi.org/10.1016/j.jsv.2010.08.041.

[17] N. Nawayseh, S. Hamdan, Apparent mass of the standing human body when using a whole-body vibration training machine: Effect of knee angle and input frequency, J. Biomech. 82 (2019) 291–298. https://doi.org/10.1016/j.jbiomech.2018.11.003.

[18] Y. Matsumoto, M.J. Griffin, Dynamic Response of the Standing Human Body Exposed To Vertical Vibration: Influence of Posture and Vibration Magnitude, J. Sound Vib. 212 (1998) 85–107.
[19] P. Lugner, H. Pacejka, M. Plöchl, Recent advances in tyre models and testing procedures, Veh. Syst. Dyn. 43 (2005) 413–426. https://doi.org/10.1080/00423110500158858.
[20] R. Lot, A motorcycle tire model for dynamic simulations: Theoretical and experimental aspects, Meccanica. 39 (2004) 207–220. https://doi.org/10.1023/B:MECC.0000022842.12077.5c.
[21] A.J.C. Schmeitz, I.J.M. Besselink, S.T.H. Jansen, Tno Mf-Swift, Veh. Syst. Dyn. 45 (2007) 121–137. https://doi.org/10.1080/00423110701725208.
[22] Comité Européen de Normalisation, Light motorized vehicles for the transportation of persons and goods and related facilities and not subject to type-approval for on- road use - Personal light electric vehicles (PLEV) - Requirements and test (EN Standard No. 17128 : 2020), (2020).
[23] International Organization for Standardization, Mechanical vibration — Road surface profiles — Reporting of measured data (ISO Standard No. 8608:2016), (2016). https://www.iso.org/standard/71202.html.
[24] M. Kučera, M. Helexa, J. Čedík, Link between static radial tire stiffness and the size of its contact surface and contact pressure, Agron. Res. 14 (2016) 1361–1371.
[25] F. Koutny, Load-deflection curves for radial tyres, Appl. Math. Model. 5 (1981) 422–427. https://doi.org/10.1016/S0307-904X(81)80025-X.
[26] S. Rapoport, J. Mizrahi, E. Kimmel, O. Verbitsky, E. Isakov, Constant and variable stiffness and damping of the leg joints in human hopping, J. Biomech. Eng. 125 (2003) 507–514. https://doi.org/10.1115/1.1590358.
[27] International Organization for Standardization, Mechanical vibration and shock — Mechanical impedance of the human hand-arm system at the driving point (ISO Standard No. 10068:2012), (2012). https://www.iso.org/standard/53714.html.